

Hidden spin liquid in an antiferromagnet: Applications to FeCrAs

Jeffrey G. Rau and Hae-Young Kee

Department of Physics, University of Toronto, Toronto, Ontario, Canada M5S 1A7

(Received 18 July 2011; published 30 September 2011)

The recently studied material FeCrAs exhibits a surprising combination of experimental signatures, with metallic, Fermi-liquid-like specific heat but resistivity showing strong nonmetallic character. The Cr sublattice possesses local magnetic moments, in the form of stacked (distorted) kagome lattices. Despite the high degree of magnetic frustration, antiferromagnetic order develops below $T_N \sim 125$ K suggesting the nonmagnetic Fe sublattice may play a role in stabilizing the ordering. From the material properties we propose a microscopic Hamiltonian for the low-energy degrees of freedom, including the nonmagnetic Fe sublattice, and study its properties using slave-rotor mean-field theory. Using this approach we find a spin-liquid phase on the Fe sublattice, which survives even in the presence of the magnetic Cr sublattice. Finally, we suggest that the features of FeCrAs can be qualitatively explained by critical fluctuations in the nonmagnetic Fe sublattice due to proximity to a metal-insulator transition.

DOI: 10.1103/PhysRevB.84.104448

PACS number(s): 71.10.Hf

I. INTRODUCTION

The ubiquity of Landau's Fermi liquid is a testament to universality in the solid state. As such, departures from these classic experimental signatures in metallic systems act as a guide to novel and interesting physics. Non-Fermi-liquid behavior appears in many strongly correlated materials such as unconventional superconductors,¹⁻³ heavy fermion materials,^{4,5} and near quantum phase transitions.^{6,7} Some routes to realize this behavior include coupling itinerant electronic systems to localized magnetic moments and through intermediate to strong electron-electron interactions. These mechanisms can give rise to characteristics and experimental signatures that do not fit neatly in the Fermi-liquid paradigm.

A recently reexamined compound, FeCrAs,⁸⁻¹⁰ provides a direct example of a material that does not fit completely within Fermi-liquid theory and combines aspects of the mechanisms discussed above. The unit cell of FeCrAs shown in Fig. 1 shows Cr and Fe form alternating two-dimensional lattices along what we will denote the c axis. Cr forms layers with the structure of a distorted kagome lattice where the Cr-Cr distances are approximately constant. The Fe layers have a more complicated structure, forming a triangular lattice of three atom units, which we will call trimers, as shown in Fig. 2. The As is interspersed throughout both the Fe and Cr layers, as well as in between. Most of the known experimental data is nicely presented in Wu *et al.*,¹⁰ which we summarize below.

The specific heat exhibits Fermi-liquid behavior at low temperatures, i.e., $C \sim \gamma T$, where the slope γ is sample dependent.¹¹ The measured linear range is roughly $T \sim 2$ –10 K. Resistivity measurements show nonmetallic behavior at low and high temperatures. In-plane (ab) and out-of-plane (c) resistivities are of the same order over the entire temperature range considered. The resistivity monotonically decreases (i.e., $d\rho/dT < 0$) as T is raised from 4 K up to ~ 800 K except for a small peak in the c -axis resistivity around $T \sim 125$ K. A low-temperature power law $\rho \sim \rho_0 - AT^\alpha$ is observed for $T \sim 80$ –10 K in both ab planes and c -axis resistivity with $\alpha \sim 0.6$ –0.7.

There is a peak in the susceptibility at $T_N \sim 125$ K indicating a magnetic transition with a lack of hysteresis pointing

to antiferromagnetic ordering. Below T_N the susceptibility is anisotropic, differing between the ab plane and the c axis. Elastic neutron scattering¹² done deep in the magnetic phase, at $T = 2.8$ K, is consistent with the antiferromagnetic order inferred from the susceptibility, signaling an ordering vector at $\vec{Q} = (\frac{1}{3}, \frac{1}{3}, 0)$, indicating ferromagnetic (stacked) order along the c axis, but with a tripled unit cell in the ab plane. While measurements of the specific heat give a result consistent with a metallic Fermi liquid, transport is unusual and deviates strongly from the classic Fermi-liquid result for metals, while being distinct from the expected result for insulators. Furthermore, this material has a frustrated magnetic sublattice that nonetheless orders at low temperatures, while the remaining sublattices show either small or no magnetic moment.^{10,12} The magnetic sublattice takes the form of a distorted kagome lattice, where even classical Heisenberg models fail to order magnetically for both the stacked^{13,14} and purely two-dimensional cases.¹⁵⁻¹⁹ Very few experiments have been carried out on FeCrAs, so theoretical models are not completely restricted. Regardless, there are a number of questions that need to be addressed, such as the nature of the stabilization of magnetic order, the cause of the very different thermodynamic and transport signals, and the role of the nonmagnetic sublattice.

The nature of the magnetic order has been recently addressed by Redpath *et al.*,²⁰ where a minimal model was proposed which suffices to explain the experimentally observed stabilization of a particular magnetic ordering vector. However, transport and thermodynamic behavior remain to be explained, along with the role of the nonmagnetic Fe sublattice. In this paper, we elaborate a microscopic route to an effective model for the compound FeCrAs, taking into account the Fe sublattice, and present a scenario to address the incongruities between the conflicting metallic, Fermi-liquid specific heat and nonmetallic transport signals. This model consists of interacting electrons of the nonmagnetic Fe sublattice coupled to magnetic moments of the magnetic Cr sublattice. Here we do not address the detailed nature of the moments themselves, treating them classically,²⁰ with the non-Fermi-liquid physics arising from strong charge

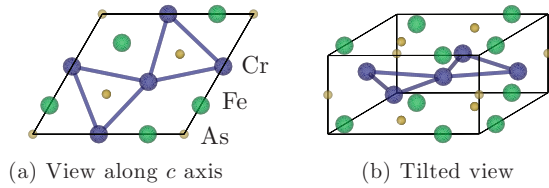


FIG. 1. (Color online) FeCrAs unit cell viewed along the c axis (left) and tilted away by 70° (right). Fe atoms are indicated in green, Cr in blue, and As in yellow.

fluctuations occurring at intermediate Hubbard coupling in the Fe sublattice. In this picture we are excluding any Kondo physics, a view supported by the experimental results. Our emphasis is on the interplay between strong charge fluctuations near the metal-insulator transition on the Fe sublattice and the magnetic order of the Cr sublattice. For this we turn to the slave-rotor method which allows access to the intermediate coupling regime and metal-insulator transition.

The structure of the paper is as follows: in Sec. II we present an argument to pass from the atomic limit through to an effective model of the electronic degrees of freedom in FeCrAs. In Sec. II D we discuss the localized moments and magnetic interactions and we present the effective Hamiltonian relevant for FeCrAs. We proceed to review the slave-rotor method in Sec. III and the assumptions and implementation of our mean-field theory in Sec. IV. In Sec. V we comment on the application of our results to FeCrAs and summarize conclusions in Sec. VI.

II. EFFECTIVE HAMILTONIAN

A. Local environments and spin states

Considering the common oxidation states of Fe we will take (in the atomic limit) Fe^{3+} as a starting point. This leaves the valence configuration being $3d^5$ for Fe^{3+} . Following the experimental data, we assume that the Fe atoms are in a low spin state, due to the lack of a detectable magnetic moment.¹² The tetrahedral arrangement of the As atoms about each Fe atom, shown in Fig. 3(a), implies a crystal field producing a splitting of the Fe d levels, shown in Fig. 4(a), with a pair of low-lying e levels and a threefold degenerate set of t_2 levels, separated by the crystal-field gap. Assuming the low spin case is relevant, the two e states are filled and there is a single electron in the t_2 triplet shown in Fig. 4(b).

The case of Cr is more complicated, as the experiments do not single out a more probable spin state. For Cr we will take an ionic charge of Cr^{2+} , giving a valence configuration of $3d^4$. A distorted octahedral environment, shown in Fig. 3(b),

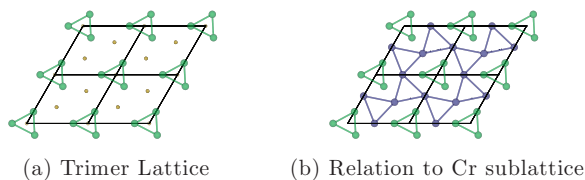


FIG. 2. (Color online) (a) The Fe sublattice with trimers shown explicitly. (b) The local environment of the trimer, with respect to the Cr sublattice.

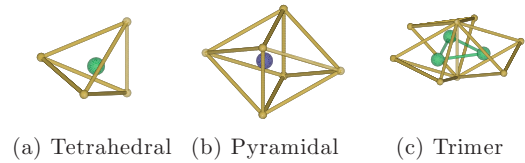


FIG. 3. (Color online) The local environments of the Fe (a), Cr (b), and trimer (c). The Fe atom is tetrahedrally coordinated and the Cr atom is approximately octahedrally coordinated. The trimer is surrounded by three tetrahedra that share a common axis.

reduces the symmetry about this site to C_{4v} , with crystal-field splittings shown in Fig. 5(a). The low spin state [shown in Fig. 5(b)] can still yield an $S = 1$ spin moment, while the high spin state has an $S = 2$ moment. In the low spin case, hopping onto the Cr^{2+} will be suppressed by the orbital repulsion, while for the high spin case the crystal-field energy will give a further suppression.

We would like to emphasize that the arguments and models presented here are underconstrained by both experimental results and first-principles electronic structure calculations.²¹ Due to this limitation the precise details could fail quantitatively, but the subsequent effective Hamiltonian appears to be robust to a variety of ionic configuration changes in the underlying model. For example, the specific oxidation state we use for the Cr will be irrelevant to our final discussion, as only the localized character is needed to capture the gross magnetic features.²⁰ With this in mind, below we present a possible route from the microscopic Hamiltonian to the effective model.

B. Iron-chromium interactions

Since the Fe-Cr distance is considerably smaller than the direct Fe-Fe distances outside the trimers and the indirect Fe-As-Cr distance, we will consider interactions induced by Fe-Cr-Fe hopping paths. First we define a simple model for an isolated Cr atom, assuming a low spin state as shown in Fig. 5(b). The local Hamiltonian for the Cr e doublet assumes the natural form

$$H_{\text{Cr}} = \Delta \sum_{j\alpha\sigma} n_{j\alpha\sigma} + U \sum_{j\alpha} n_{j\alpha\uparrow} n_{j\alpha\downarrow} - J \sum_j \left(\sum_{\alpha} \vec{S}_{j\alpha} \right)^2, \quad (1)$$

where $n_{j\alpha\sigma} = e_{j\alpha\sigma}^\dagger e_{j\alpha\sigma}$ is the number operator for the state in the doublet α . We have denoted the atomic potential as Δ ,

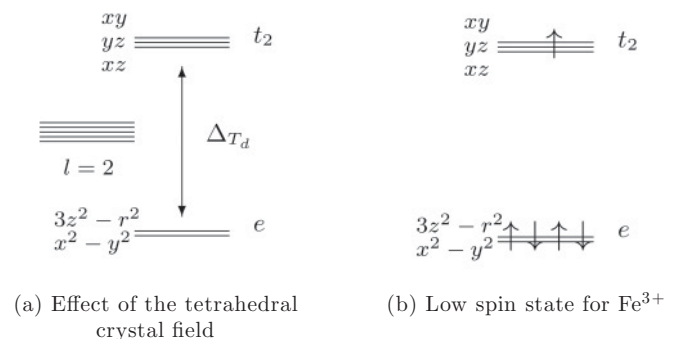


FIG. 4. The effect of the crystal field on the Fe^{3+} ion. The local symmetry about this site is tetrahedral; that is, the group T_d .

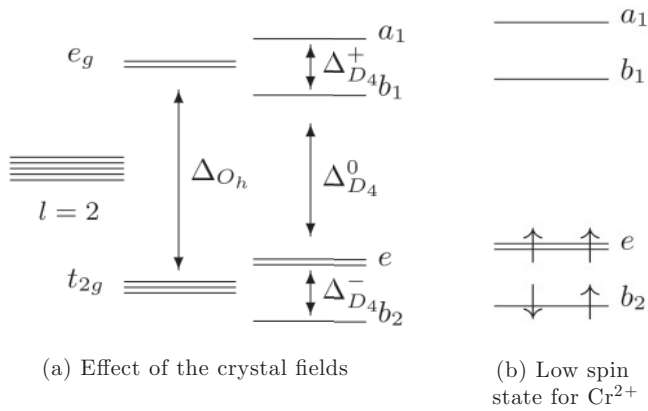


FIG. 5. The effect of crystal fields on the Cr^{2+} ion. The Cr ion is biased toward one direction of the octahedron. This reduces the symmetry to the group C_{4v} .

the intraorbital repulsion as U , and the Hund's coupling as J . Allowing for hopping between Fe and Cr, we include the term

$$H_{\text{Cr-Fe}} = - \sum_{ij\sigma\alpha} t_{ij}^{\alpha} d_{i\sigma}^{\dagger} e_{j\alpha\sigma} + \text{H.c.}, \quad (2)$$

where i runs over the orbitals on sites connected to the Cr atom at site j and d is the annihilation operator on the Fe site i . Integrating out all of the high-energy degrees of freedom on the Cr atom, the ground state for sufficiently large J is given by the doubly occupied, $S = 1$ triplet states, which we denote by $|t_{ja}\rangle$ with $a = 0, \pm$. Noting that $H_{\text{Cr-Fe}}$ does not connect triplet to triplet states, as it changes the electron number on the Cr atom we can formulate the effective Hamiltonian following

$$H_{\text{eff}} = P_t H_{\text{Cr-Fe}} (E_0 - H_{\text{Cr}})^{-1} H_{\text{Cr-Fe}}^{\dagger} P_t, \quad (3)$$

where E_0 is the triplet energy and $P_t = \sum_{ja} |t_{ja}\rangle \langle t_{ja}|$ projects onto the triplet subspace. Carrying out the expansion of the effective Hamiltonian, denoting the spin operators on the Cr and Fe atoms as \vec{S}_i and $\frac{1}{2} d_i^{\dagger} \vec{\sigma} d_i$, respectively, our full effective Hamiltonian is given by

$$H_{\text{eff}} = - \sum_{ijl} \frac{1}{W} \left(\sum_{\alpha} t_{ij}^{\alpha} (t_{lj}^{\alpha})^* \right) d_i^{\dagger} (1 - \vec{\sigma} \cdot \vec{S}_j) d_l, \quad (4)$$

where

$$\frac{1}{W} = \frac{U + \frac{5J}{2}}{\Delta^2 + \left(\frac{5J}{4}\right)^2 + U\left(\frac{5J}{4} - \Delta\right)} > 0. \quad (5)$$

For $i = l$ this represents an antiferromagnetic exchange between the Fe and Cr atoms, while $i \neq l$ presents a spin-dependent hopping term, nonzero for both intratrimer and intertrimer hopping paths. Based on overlap of the orbital wave functions, we assume that the hopping $\sum_{\alpha} |t_{ij}^{\alpha}|^2$ is dominant for $i = l$ and independent of the orbitals, leading to the effective exchange Hamiltonian

$$H_{\text{eff}}^{\text{exch}} = \sum_{ij} \frac{1}{W} \left(\sum_{\alpha} |t_{ij}^{\alpha}|^2 \right) d_i^{\dagger} (\vec{\sigma} \cdot \vec{S}_j) d_i, \quad (6)$$

up to a shift of the chemical potential. For future use, we will denote the effective exchange as

$$J_K = \frac{1}{W} \sum_{\alpha} |t_{ij}^{\alpha}|^2 > 0. \quad (7)$$

C. Trimer approximation for Fe

From the interatomic distances we expect that the Fe-Fe atoms in the trimer structure are tightly coupled. We can take advantage of this by grouping the degrees of freedom in the trimer into a single unit and formulating the rest of our theory in terms of these variables. This process is similar to the treatment of the pairs of molecules as the effective degrees of freedom frequently employed in studies of organic superconductors.³ This assumes the energy scales for interactions and intertrimer hopping matrix elements are small relative to the intratrimer hoppings. In addition, we require that the tetrahedral crystal-field splitting be much larger than our intraorbital interactions (this is the low spin assumption) and both the intra- and intertrimer hopping elements.

With this in mind, let us find the low-energy degrees of freedom of a trimer, keeping only the three-site cluster. Considering the C_3 symmetry, there are four possibilities for the degeneracies of the two lowest levels, leading to either a half- or quarter-filled band as the relevant states (assuming all gaps are large compared to the relevant energy scales). Motivated by the Slater-Koster argument in the Appendix, we start with a model for the xy , xz , and yz orbitals of the trimer:

$$H_{\text{trimer}} = - \sum_{(ij)} d_i^{\dagger} \begin{pmatrix} 0 & t_{xz,yz} & 0 \\ t_{xz,yz} & 0 & 0 \\ 0 & 0 & t_{xy,xy} \end{pmatrix} d_j, \quad (8)$$

where $d_i^{\dagger} = (d_{i,xz}^{\dagger} \ d_{i,yz}^{\dagger} \ d_{i,xy}^{\dagger})$ and $i, j = 1, 2, 3$ are the sites in the trimer. The xy part is just a simple three-site chain with a ground state at $-2t_{xy,xy}$ and a pair of excited levels at $t_{xy,xy}$. For the xz and yz orbitals we can diagonalize H_{trimer} by changing the basis:

$$d_{i,+} = \frac{1}{\sqrt{2}} (d_{i,xz} + d_{i,yz}), \quad (9)$$

$$d_{i,-} = \frac{1}{\sqrt{2}} (d_{i,xz} - d_{i,yz}). \quad (10)$$

This gives a pair of decoupled three-site chains with hoppings $\pm t_{xz,yz}$ and thus energy levels of $\pm 2t_{xz,yz}$ and $\mp t_{xz,yz}$. When $\frac{1}{2} t_{xy,xy} < t_{xz,yz} < 2t_{xy,xy}$ a single half-filled level in the trimer, symmetric under permutations of the three sites, is realized. Ignoring all of the other matrix elements in the complete hopping matrix, we find (see the Appendix)

$$t_{xz,yz} \sim \frac{1}{32} (7t_{\delta} - 16t_{\pi} + 9t_{\sigma}), \quad (11)$$

$$t_{xy,xy} \sim \frac{1}{64} (49t_{\delta} - 12t_{\pi} + 3t_{\sigma}). \quad (12)$$

A more complete model would include mixing between all three orbitals but the qualitative picture should remain the same. The naive choice of $t_{\delta} < t_{\pi} < t_{\sigma}$ seems to select the case of $t_{xy,xy} > t_{xz,yz}$ and thus the single occupied band has d_+ character (shown in Fig. 6). Note the gap between the

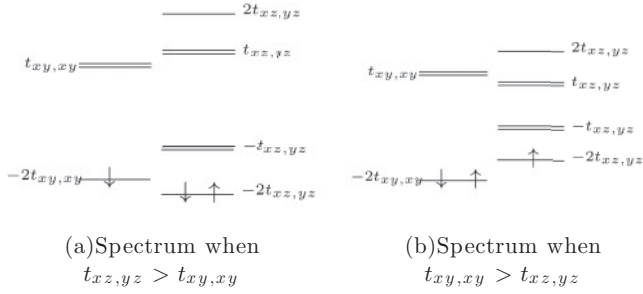


FIG. 6. The two cases that give rise to a half-filled band, with $t_{xy,xy} \approx t_{xz,yz}$. We can either have a band with (a) d_{xy} character or with (b) d_+ character.

occupied level and the half-filled level is given by

$$\Delta_{\text{trimer}} \sim 2|t_{xy,xy} - t_{xz,yz}| = \frac{5}{64} |7t_\delta + 4t_\pi - 3t_\sigma|, \quad (13)$$

and must be fairly large to ensure that the trimer approximation is valid. We emphasize that regardless of the exact details of these hoppings the qualitative picture will remain, as long as this half-filling is found such as for Fe^{3+} . Other oxidation states will give a different relevant molecular orbital, possibly with extra orbital degeneracy, and could change the picture presented here.

D. Effective Hamiltonian and magnetic interactions

The gross magnetic structure of FeCrAs can be captured by a classical model of localized moments interacting with the Fe sublattice via a simple exchange.²⁰ The utility of the classical model for the moments is also supported by the fact that Kondo-like signatures are absent in the experimental data. Furthermore, due to the uniform character of the relevant trimer states and the assumption of equal exchanges between Cr and different Fe orbitals, the effective exchange between the Cr and the trimers will be equal and between all of the Cr in the surrounding hexagons in the layers above and below. We thus take our Hamiltonian to have the form

$$H = -t \sum_{\langle ij \rangle \in ab} \sum_{\sigma} c_{i\sigma}^\dagger c_{j\sigma} - t' \sum_{\langle ij \rangle \in c} \sum_{\sigma} c_{i\sigma}^\dagger c_{j\sigma} + U \sum_i n_{i\uparrow} n_{i\downarrow} + \frac{J_K}{2} \sum_{i,a \in \circ i} (c_i^\dagger \vec{\sigma} c_i) \cdot \vec{S}_a + J_H \sum_{\langle ab \rangle} \vec{S}_a \cdot \vec{S}_b, \quad (14)$$

where the low-energy degrees of freedom on the trimers are denoted using the operators $c_{i\sigma}^\dagger, c_{i\sigma}$ and the classical Cr spins are denoted as \vec{S}_a . The trimer sublattice is afforded hoppings t and t' which originate from direct overlaps between trimers (or indirectly via Cr or As) in the ab planes and along the c axis, respectively. Here we denote sites on the Fe sublattice as i and j , while sites on the Cr sublattice are denoted as a and b . The notation $a \in \circ i$ indicates that the sum on the Cr sublattice is over sites in the hexagon that surround the trimer at i on the Fe sublattice. Furthermore, $\langle ij \rangle \in ab, c$ denotes bonds in the ab plane or c direction, respectively. The interactions are given as follows: U is the intratrimer repulsion, inherited from the Fe atoms, J_K is the Fe-Cr exchange and J_H is the Cr-Cr exchange. This is shown in Fig. 7. In this Hamiltonian the Cr spins appear as an effective magnetic field for the trimers, which we will denote as $\vec{h}_i = \sum_{a \in \circ i} \vec{S}_a$.

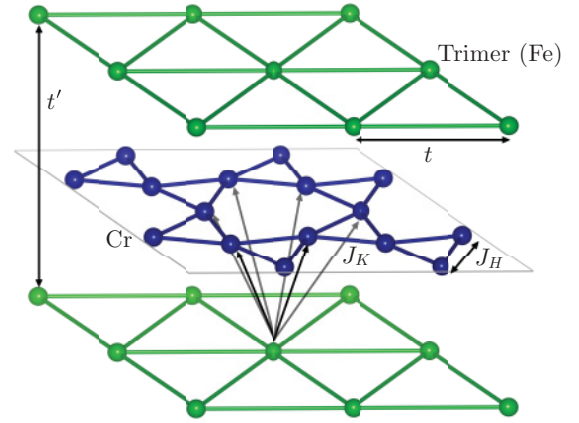


FIG. 7. (Color online) The hoppings and exchanges for the model Hamiltonian in Eq. (14). The notations are discussed in the text.

In the large U limit, where $U \gg t$ and $t^2/U, (t')^2/U \ll J_K, J_H$, this model should reproduce the model studied in Ref. 20, and thus their classical results provide a useful point of comparison for our large U/t behavior. To attack the intermediate U/t regime we will use a slave-rotor approach, reviewed in the following section.

III. SLAVE ROTORS

For completeness and standardization of notation, we review the general properties of two-dimensional rotors and follow with a discussion of the slave-particle representation that bears their name.²²

A rotor in two dimensions is an object that possesses only angular momentum, prototypically of the form $H \propto L^2$, where L is the angular momentum operator about some axis, say the \hat{z} axis. We classify states by the eigenstates of the L operator, $L|n\rangle = n|n\rangle$, where n is an integer. Raising and lowering operators are defined as

$$U^\dagger |n\rangle = |n+1\rangle, \quad U |n\rangle = |n-1\rangle,$$

where U is a unitary operator. From this definition it is simple to show that L and U satisfy the commutation relations,

$$[L, U] = -U, \quad [L, U^\dagger] = U^\dagger.$$

Since U is unitary it can be written as $U = \exp(-i\theta)$, where $\theta^\dagger = \theta$ and one can show that this implies the canonical commutation relation $[\theta, L] = i$, showing that L and θ are canonically conjugate variables.

To use these rotors as a slave particle we associate the local electron basis with the product of the states of slave fermion and the states of an $O(2)$ rotor,

$$\begin{aligned} |0\rangle &= |0\rangle_f | +1\rangle_\theta, \\ |\uparrow\rangle &= |\uparrow\rangle_f |0\rangle_\theta, \\ |\downarrow\rangle &= |\downarrow\rangle_f |0\rangle_\theta, \\ |\uparrow\downarrow\rangle &= |\uparrow\downarrow\rangle_f | -1\rangle_\theta. \end{aligned}$$

The slave fermion is called a spinon and spinon states are denoted by an f subscript. The slave rotor will be referred to as a rotor and a θ subscript will be used to denote rotor states.

The natural interpretation is to have the spinon be neutral and the rotor carry the charge of the electron, thus explicitly separating the spin and charge degrees of freedom. Having expanded our local Hilbert space, a constraint is required to remove the unphysical states. The four physical states above are characterized by

$$L_i + \sum_{\sigma} n_{i\sigma}^f = 1,$$

where L_i is the rotor angular momentum operator and $n_{i\sigma}^f$ is the spinon number operator. This is the Hilbert space constraint. The electron operators can therefore be expressed as

$$c_{i\sigma} = f_{i\sigma} e^{i\theta_i},$$

where $\exp(-i\theta_i)$ is the rotor-lowering operator and $f_{i\sigma}, f_{i\sigma}^{\dagger}$ are the fermionic spinon operators. Using this representation the electronic Hamiltonian for the trimers (14) is written as

$$\begin{aligned} H_e = & -t \sum_{(ij) \in ab} \sum_{\sigma} f_{i\sigma}^{\dagger} f_{j\sigma} e^{-i(\theta_i - \theta_j)} \\ & -t' \sum_{(ij) \in c} \sum_{\sigma} f_{i\sigma}^{\dagger} f_{j\sigma} e^{-i(\theta_i - \theta_j)} \\ & + \frac{U}{2} \sum_i L_i(L_i - 1) + \frac{J_K}{2} \sum_{i, a \in \square_i} (f_i^{\dagger} \vec{\sigma} f_i) \cdot \vec{S}_a. \end{aligned}$$

The Hubbard term is now a kinetic term for the rotors, so the complexity of the Hubbard interaction has been moved to the hopping term and the constraint. We note that the Fe-Cr coupling term only involves the spinon degrees of freedom.

IV. MEAN-FIELD THEORY

We approach this problem using mean-field theory. For simplicity we take the perspective of Florens and Georges,²² first decoupling the hopping term into

$$f_{i\sigma}^{\dagger} f_{j\sigma} e^{-i(\theta_i - \theta_j)} \approx \chi_{ij} e^{-i(\theta_i - \theta_j)} + B_{ij} f_{i\sigma}^{\dagger} f_{j\sigma} - \chi_{ij} B_{ij},$$

where we have introduced the mean fields $\chi_{ij} = \frac{1}{2} \sum_{\sigma} \langle f_{i\sigma}^{\dagger} f_{j\sigma} \rangle$ and $B_{ij} = \langle e^{-i(\theta_i - \theta_j)} \rangle$. Note that we have assumed that χ_{ij} is independent of spin. To handle the constraint we treat it both on average in space and on average in our states. For the case of half-filling this leads to the two conditions

$$\sum_i \langle L_i \rangle = 0, \quad \sum_{i\sigma} \langle n_{i\sigma}^f \rangle = 1.$$

Note that applying this on average in space prohibits us from considering charge ordering in our calculations. To enforce these constraints we introduce chemical potentials for the rotors and for the spinons, μ_L and μ_f , respectively. This leads to two independent Hamiltonians which only talk to each other through the mean fields χ_{ij} and B_{ij} ,

$$\begin{aligned} H_f = & - \sum_{(ij)\sigma} (t_{ij} B_{ij} + \mu_f \delta_{ij}) f_{i\sigma}^{\dagger} f_{j\sigma} \\ & + \frac{J_K}{2} \sum_{i, a \in \square_i} (f_i^{\dagger} \vec{\sigma} f_i) \cdot \vec{S}_a, \end{aligned}$$

$$H_L = -2t \sum_{(ij)} \chi_{ij} e^{-i\theta_i} e^{i\theta_j} + \frac{U}{2} \sum_i (L_i^2 - \mu_L L_i),$$

where we have introduced t_{ij} which is equal to t on the in-plane triangular bonds and equal to t' on the out-of-plane bonds. While the spinon Hamiltonian can be treated using mean-field theory, the rotor Hamiltonian needs a different strategy.

Two approaches for the rotor Hamiltonian have been used in the literature: a self-consistent cluster approach²³ and a bosonic approach.²² Taking the bosonic approach, which is most simply tackled using a path-integral formulation, the imaginary time action takes the form

$$\begin{aligned} S(\theta, L) = & \int_0^{\beta} d\tau \left[\sum_i \left(i L_i \partial_{\tau} \theta_i + \frac{U}{2} L_i^2 \right) \right. \\ & \left. - 2 \sum_{ij} t_{ij} \chi_{ij} e^{-i\theta_i} e^{i\theta_j} \right], \end{aligned}$$

where μ_L is chosen to eliminate the linear terms in S . Due to the symmetry of the action this guarantees that $\langle L_i \rangle = 0$. Next, we integrate out L to get the following action:

$$S(\theta) = \int_0^{\beta} d\tau \left[\frac{1}{2U} \sum_i (\partial_{\tau} \theta_i)^2 - 2 \sum_{(ij)} t_{ij} \chi_{ij} e^{-i\theta_i} e^{i\theta_j} \right]. \quad (15)$$

We write this using a bosonic variable $\phi_i = e^{i\theta_i}$ subject to the constraint that $|\phi_i|^2 = 1$, giving

$$\begin{aligned} S(\bar{\phi}, \phi; \lambda) = & \int_0^{\beta} d\tau \left[\frac{1}{2U} \sum_i |\partial_{\tau} \phi_i|^2 - i \sum_i \lambda_i \right. \\ & \left. + \sum_{(ij)} (i \lambda_i \delta_{ij} - 2 t_{ij} \chi_{ij}) \bar{\phi}_i \phi_j \right], \quad (16) \end{aligned}$$

where λ is an auxiliary field introduced to enforce the constraint. Treating this new constraint in saddle-point approximation, the solution of the bosonic part of the Hamiltonian is reduced to solving this saddle-point equation and a free bosonic problem. These saddle-point equations simply fix the boson number at each site to one.

We assume a uniform state on the Fe sublattice, by considering $\chi_{ij} \equiv \chi$ and $B_{ij} \equiv B$ in plane, with $\chi_{ij} = \alpha \chi$ and $B_{ij} = \alpha B$ out of plane, where α is chosen so that we smoothly match the noninteracting limit.¹ For the Cr spins it is natural to assume that the periodicity is that found by experiments^{10,12} and previous classical calculations,²⁰ with wave vector $(1/3, 1/3, 0)$. Within this space of magnetic states, we consider only canted classical ground states; that is, states where the in-plane components in each triangle are at 120° apart, but they are tilted out of plane by a canting angle ψ . These states interpolate between a subset of the ground states for $J_H \gg J_K$ at $\psi = 0$ and the ferrimagnetic state²⁰ valid for $J_K \gg J_H$ with $\psi = \pi/2$. Among these states one can see that only those with a finite moment, as one sums around a hexagon in the kagome lattice, will be favored due to the J_K interaction. With these constraints we only have a

¹More general ansatzes could be employed while maintaining uniformity, such as varying the phases of χ and B over the tripled unit cell or including spin-dependent χ . For simplicity we leave these considerations for future work.

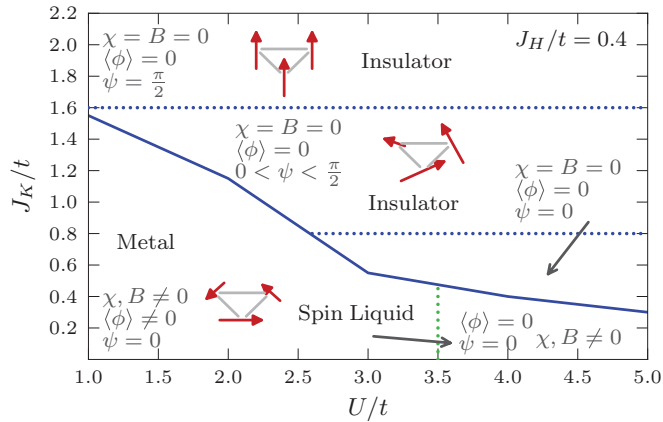


FIG. 8. (Color online) Phase diagram as a function of J_K/t and U/t for the value $J_H/t = 0.4$. The inset diagrams show a sample of the Cr spin configuration on one of the kagome triangles. χ and B are the slave-rotor mean-field parameters, $\langle\phi\rangle$ is the rotor condensate, and ψ is the Cr canting angle (see text).

single set of magnetic states to consider parametrized by the canting angle ψ . Under these assumptions the trimer feels the following effective magnetic field (defined as $\vec{h}_i = \sum_{a \in \odot_i} \vec{S}_a$) after summing around the hexagon

$$\vec{h}_i = 6S \cos \psi [\cos(\vec{Q} \cdot \vec{r}_i) \hat{x} + \sin(\vec{Q} \cdot \vec{r}_i) \hat{y}] + 12S \sin \psi \hat{z},$$

where $\vec{Q} = (1/3, 1/3, 0)$ and S is the magnitude of the Cr moment. Note the factor of 2 between the in-plane and out-of-plane components due to the partial cancellation as we sum around the hexagon. The phase diagram for $J_H/t = 0.4$ is shown in Fig. 8, and demonstrates the full range of phases.

There are three distinct phases shown in these phase diagrams. At low J_K/t and U/t we find a metallic phase on the Fe sublattice with zero canting angle (i.e., in plane, 120° ordering) on the Cr sublattice. This metallic state is characterized by condensation of the bosonic degree of freedom ($\langle\phi\rangle \neq 0$) and a uniform, real $\chi_{ij} = |\chi|$ implying the existence of an electron Fermi surface and gapless charge excitations. Furthermore, the Fe trimers have an induced moment (antiferromagnetically) following the Cr moment. This moment scales with J_K/t , and thus will be small so long as J_K/t is. As we increase U/t and keep J_K/t small, we find a metal-insulator transition near $U_c/t \approx 3.5$ into a uniform, $U(1)$ spin-liquid (SL) phase. The metal-insulator boundary is very flat, as seen in Fig. 8, since under the mean-field ansatz we have employed the critical U is only a function of χ , which changes only by a small amount as we increase J_K (below the jump into the paramagnet phase). This SL phase is also characterized by a uniform, real χ_{ij} but gapped bosons ($\langle\phi\rangle = 0$), meaning the existence of a spinon Fermi surface but gapped charge excitations. This insulating phase carries the induced moment as in the metallic phase, with the magnitude also being proportional to J_K/t . In both the metallic and insulating phases as J_K/t is increased (but remains small) the χ -order parameter decreases toward zero.

From the spin-only model of Ref. 20 (accounting for the differing normalizations) one expects that for large U/t the canting angle will become nonzero at $J_K = 2J_H$ and saturate at $J_K = 4J_H$ as one sees in Fig. 8. We find that the uniform spin liquid does not support a nonzero canting angle. By this we

mean that as J_K/t is increased, the canting angle remains zero until some critical J_K/t , wherein the spin liquid is replaced by the canted antiferromagnet (AF) with $\chi = B = 0$. The converse is not true, as can be seen in Fig. 8. We see that the spin-liquid phase can be destroyed before the onset of the canted magnetic state, leaving a window where we have a simple insulating, in-plane antiferromagnet. Once inside this canted AF phase with $\chi = B = 0$, the canting angle increases with J_K/t until it becomes saturated and we enter a ferrimagnetic phase, with a net magnetic moment. The key feature of the phase diagrams we want to emphasize is that for a variety of values of J_H and for small J_K this spin-liquid state is stable and does not coexist with a finite canting.

V. DISCUSSION

To discuss the applications of this to FeCrAs the effects of fluctuations must be taken into account near the metal-insulator transition. These include both charge and gauge degrees of freedom and are treated in detail in the work of Podolsky *et al.*²⁴ In this work it is found that there are two relevant temperature scales T^* and T^{**} that determine the qualitative features of the thermodynamic and transport properties. These temperature scales vanish as one approaches the critical point separating the metal and insulator. At temperatures above these scales the specific heat has weak logarithmic corrections

$$C \sim T \ln \ln(1/T), \quad (17)$$

while the conductivity has a strong temperature dependence. Specifically, writing $\sigma = \sigma_f + \sigma_b$, where σ_f is the spinon conductivity and σ_b is boson conductivity, under the assumption of weak disorder we have $\sigma_f \sim \sigma_f^{\text{imp}}$ due to impurity scattering and

$$\sigma_b \sim T \ln^2(1/T). \quad (18)$$

This implies that the effects of the fluctuations on the specific heat are much more difficult to discern experimentally than the effect on the resistivity, which will be a monotonically decreasing function of T , as seen in the experiments on FeCrAs. This is a possible scenario for FeCrAs where a nearly linear specific is observed, as these logarithmic corrections would only be visible over large temperature ranges, where other contributions would begin to dominate and wash out the signature. This is also consistent with the magnetoresistance measurements,¹⁰ where no change is seen in the low-temperature resistivity under magnetic fields up to 8 T, as the magnetic field would only couple weakly to the rotor fluctuations.

A method to test this hypothesis experimentally would be a study of the pressure dependence of the transport and thermodynamic properties. Naively one expects that the application of pressure should drive the material through the metal-insulator transition, into the quantum critical metal and eventually into a Fermi-liquid phase. Under our scenario, this could, in principle, be visible as the development of a maximum in the resistivity at low temperatures as the pressure is increased. Furthermore, the specific heat should be relatively unaffected, still only being renormalized by a logarithmic term.

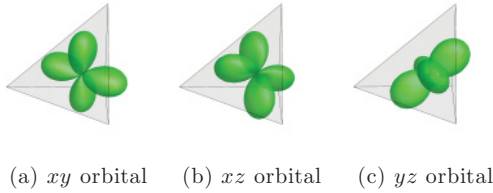


FIG. 9. (Color online) The orbitals of the t_2 level, rotated along the local axes of an As tetrahedron.

The limitations of the current study deserve some discussion as they lead to future directions. Due to the natural ansatz used in the slave-rotor study, a number of nontrivial spin-liquid states have been excluded from the analysis, such as those with a nontrivial phase structure or those that break translational symmetry.²⁵ A full exploration of the possible phases in this model could yield useful insights for FeCrAs. Another aspect of this problem that requires future work is the inclusion of quantum effects in the description of the Cr spins, leading to a Kondo-Heisenberg model with strong interactions for the conduction electrons. While the addition of frustrating interactions for the Kondo spins has attracted attention recently,^{26,27} the inclusion of electronic interactions is largely unaddressed (particularly with frustration on the conduction electrons) and is an interesting, but highly nontrivial, question for future study.

VI. SUMMARY

In this paper we have presented and motivated a minimal model for the low-energy degrees of freedom in the compound FeCrAs. Starting from the crystal structure and using the experimental facts, we have argued that the magnetic degrees of freedom are well described by a set of classical, localized moments and the electronic degrees of freedom take the form of a half-filled Hubbard model on the trimer sublattice. The coupling between these two subsystems stabilizes a definite magnetic order on the localized moments despite the high degree frustration. To explain the thermodynamic and transport properties of this material at low temperatures we propose that the electrons residing on the Fe trimers could be close to a quantum critical point separating metallic and insulating phases. The charge fluctuations associated with these critical points strongly renormalize the transport properties but provide only small corrections to the thermodynamics, qualitatively consistent with the experimental results on FeCrAs. Finally, we have discussed unexplored experi-

mental consequences of this proposal and future directions for theoretical work.

ACKNOWLEDGMENTS

We thank J. Hopkinson, F. Tafti, S. Julian, Y. B. Kim, and Y. J. Kim for useful discussions. This research was supported by NSERC of Canada and the Canada Research Chair program.

APPENDIX: HOPPING INTEGRALS

We first consider direct hopping between the Fe atoms in a trimer. The t_2 level is composed of xz , yz , and xy orbitals with respect to the canonical choice of tetrahedron axes. Rotating these into the axes of a tetrahedron in a trimer, the orbitals are oriented as shown in Fig. 9.

From Fig. 9 one can estimate that the only significant hoppings would be between $xy - xy$, $xz - yz$, and $yz - xz$. One can approach this more quantitatively using the ideas of Slater-Koster²⁸ theory to compute the orbital overlaps in terms of rotation matrices and irreducible overlaps. We identify the vector connecting two sites in a trimer \hat{a} as $(\hat{x} + \sqrt{3}\hat{y})/2$, giving the (Euler) representation $R = R_z(0)R_y(-\frac{\pi}{2})R_z(-\frac{\pi}{3})$. The rotation that takes our tetrahedron into the proper axes is given as $R_T = R_z(-\frac{\pi}{2})R_y(\frac{\pi}{2})R_z(\frac{\pi}{4})$ giving the transformation to local axes R_T and $R_z(\frac{2\pi}{3})R_T$ for the neighboring tetrahedron in the trimer. This reduces the number of parameters to three, given by overlaps of $l = 2, m = 0, \pm 1, \pm 2$ orbitals displaced along the \hat{z} direction, which we will denote as t_σ , t_π , and t_δ , respectively. The hopping matrix in the basis of xz , yz , and xy is then given by

$$\frac{1}{32} \begin{bmatrix} t_\delta - 8t_\pi - 9t_\sigma & 7t_\delta - 16t_\pi + 9t_\sigma & \sqrt{\frac{3}{2}}(-7t_\delta - 4t_\pi + 3t_\sigma) \\ 7t_\delta - 16t_\pi + 9t_\sigma & t_\delta - 8t_\pi - 9t_\sigma & \sqrt{\frac{3}{2}}(-7t_\delta + 4t_\pi - 3t_\sigma) \\ \sqrt{\frac{3}{2}}(7t_\delta + 4t_\pi - 3t_\sigma) & \sqrt{\frac{3}{2}}(-7t_\delta - 4t_\pi + 3t_\sigma) & \frac{1}{2}(49t_\delta - 12t_\pi + 3t_\sigma) \end{bmatrix}.$$

Considering the orbitals at atomic separations, we expect t_σ and t_δ are positive with t_π negative. The simplest ansatz to try is $t_\sigma = t_\delta = -t_\pi \equiv t$. This gives

$$t \begin{pmatrix} 0 & 1 & 0 \\ 1 & 0 & 0 \\ 0 & 0 & 1 \end{pmatrix}, \quad (\text{A1})$$

as one might guess by looking at the orbital overlaps in the rotated axes. Varying the numerical values for the irreducible hopping parameters around this point gives qualitatively the same picture as this simple case, justifying our naive guess.

¹P. A. Lee, N. Nagaosa, and X.-G. Wen, *Rev. Mod. Phys.* **78**, 17 (2006).

²E. Abrahams and Q. Si, *J. Phys.: Condens. Matter* **23**, 223201 (2011).

³B. J. Powell and R. H. McKenzie, *Rep. Prog. Phys.* **74**, 056501 (2011).

⁴G. R. Stewart, *Rev. Mod. Phys.* **56**, 755 (1984).

⁵G. R. Stewart, *Rev. Mod. Phys.* **73**, 797 (2001).

⁶S. L. Sondhi, S. M. Girvin, J. P. Carini, and D. Shahar, *Rev. Mod. Phys.* **69**, 315 (1997).

⁷H. v. Löhneysen, A. Rosch, M. Vojta, and P. Wölfle, *Rev. Mod. Phys.* **79**, 1015 (2007).

⁸M. Nylund, M. Roger, J. Senateur, and R. Fruchart, *J. Solid State Chem.* **4**, 115 (1972).

⁹R. Fruchart, *Ann. Chim. (Paris)* **7**, 563 (1982).

¹⁰W. Wu, A. McCollam, I. Swainson, P. M. C. Rourke, D. G. Rancourt, and S. R. Julian, *Europhys. Lett.* **85**, 17009 (2009).

¹¹W. L. Wu, A. McCollam, I. P. Swainson, and S. R. Julian, *Solid State Phenom.* **170**, 276 (2011).

- ¹²I. P. Swainson, W. Wu, A. McCollam, and S. R. Julian, *Can. J. Phys.* **88**, 701 (2010).
- ¹³M. Zelli, K. Boese, and B. W. Southern, *Phys. Rev. B* **76**, 224407 (2007).
- ¹⁴D. Schmalfuß, J. Richter, and D. Ihle, *Phys. Rev. B* **70**, 184412 (2004).
- ¹⁵J. T. Chalker, P. C. W. Holdsworth, and E. F. Shender, *Phys. Rev. Lett.* **68**, 855 (1992).
- ¹⁶D. A. Huse and A. D. Rutenberg, *Phys. Rev. B* **45**, 7536 (1992).
- ¹⁷J. N. Reimers and A. J. Berlinsky, *Phys. Rev. B* **48**, 9539 (1993).
- ¹⁸A. Chubukov, *Phys. Rev. Lett.* **69**, 832 (1992).
- ¹⁹A. B. Harris, C. Kallin, and A. J. Berlinsky, *Phys. Rev. B* **45**, 2899 (1992).
- ²⁰T. E. Redpath, J. M. Hopkinson, A. A. Leibel, and H.-Y. Kee, e-print arXiv:1105.3974v1.
- ²¹S. Ishida, T. Takiguchi, S. Fujii, and S. Asano, *Physica B: Condens. Matter* **217**, 87 (1996).
- ²²S. Florens and A. Georges, *Phys. Rev. B* **70**, 035114 (2004).
- ²³E. Zhao and A. Paramekanti, *Phys. Rev. B* **76**, 195101 (2007).
- ²⁴D. Podolsky, A. Paramekanti, Y. B. Kim, and T. Senthil, *Phys. Rev. Lett.* **102**, 186401 (2009).
- ²⁵J. G. Rau and H.-Y. Kee, *Phys. Rev. Lett.* **106**, 056405 (2011).
- ²⁶P. Coleman and A. Nevidomskyy, *J. Low Temp. Phys.* **161**, 182 (2010).
- ²⁷S. Yamamoto and Q. Si, *J. Low Temp. Phys.* **161**, 233 (2010).
- ²⁸J. C. Slater and G. F. Koster, *Phys. Rev.* **94**, 1498 (1954).